Journal of Fluorescence (2019) 29:853–864
https://doi.org/10.1007/s10895-019-02390-4

ORIGINAL ARTICLE

Fluorescent Carbon Dots from *Nerium oleander*: Effects of Physical Conditions and the Extract Types

Sinem Simsek[1] · Melis Ozge Alas[2] · Belma Ozbek[1] · Rukan Genc[2]

Received: 21 February 2019 / Accepted: 6 May 2019 / Published online: 18 June 2019

Abstract

In this original research, the synthesis of carbon nanodots (CDs) from two different solvent extracts of *Nerium oleander* by the thermal method was investigated under various physical conditions such as pH, reaction temperature, ionic strength, and surface passivation agent (polyethylene glycol, PEG) presence in the reaction media. The effects of extract types and physical conditions on CDs formation were characterized by UV-Visible spectrophotometry, fluorescence spectrophotometry, Fourier transform infrared spectroscopy and dynamic light scattering analysis. Fluorescent CDs were obtained from PEG included reaction media. Additionally, the enhanced fluorescence intensity correlated with ascending reaction temperature was reported. The hydrodynamic particle size of CDs in aqueous solution was determined between ~1 and 235 nm with negative surface potential in the range of −6 mV and −28 mV. Moreover, CDs synthesized from aqueous extract mostly resulted in smaller size than that of ethanol extract based ones. The impact of surface passivation with PEG on the fluorescence feature of CDs was verified. For the relevant extracts of Oleander, CDs synthesized from PEG included formulations at pH 5 and NaCl free reaction media found as better alternatives than CDs synthesized under other conditions taking account their effect on fluorescence feature, hydrodynamic size and etc.

Keywords Carbon nanodot · *Nerium oleander* · Fluorescent nanoparticles · Green synthesis · Thermal synthesis

Introduction

Carbon nanodots have been researched due to their superior physical properties as thermal and electrical conductivity, high mechanical strength, optic and fluorescence features, photostability and etc. since the first report on their synthesis in 2004 [1–12]. Carbon nanoparticles can be used in bio-imaging, drug delivery, optoelectronics, solar cells, photocatalyst, photodetectors and other biological applications [8, 13–23]. There are various options for CDs synthesis as laser ablation [2, 5, 24–28], electrochemical [5, 25, 27, 29] or oxidative acid treatment [7, 30, 31], ultrasound [32–34]. Besides, the methods like thermal [3, 35, 36], hydrothermal [27, 37, 38] and microwave/microwave assisted [27, 39–41] synthesis are fast, easier, cheaper and environmentally friendly alternatives. To minimize the utilization of chemicals during CDs synthesis and to decrease the process costs, the utilization of organic materials as a carbon source has been preferred. Nanoparticles synthesis from natural sources have been reported widely for years [38, 42–45] and recently, the studies on the synthesis of CDs from plants have been proceeding [6, 37, 46–52].

Electronic supplementary material The online version of this article (https://doi.org/10.1007/s10895-019-02390-4) contains supplementary material, which is available to authorized users.

✉ Belma Ozbek
bozbek@yildiz.edu.tr

✉ Rukan Genc
rukangnc@gmail.com

Sinem Simsek
sinemsimsekk@gmail.com

Melis Ozge Alas
melis_alas@hotmail.com

[1] Department of Chemical Engineering, Faculty of Chemical and Metallurgical Engineering, Yildiz Technical University, Esenler, 34210 Istanbul, Turkey

[2] Department of Chemical Engineering, Faculty of Engineering, Mersin University, Yenisehir, 33343 Mersin, Turkey

The photoluminescence is one of the most remarkable features of CDs. CDs have considerable photostability along with the sustained excitation and this makes them excellent candidates for bio-imaging. Despite CDs are similar to inorganic fluorescent semiconductor nanoparticles, optical properties and chemical/photochemical stability of CDs provide advantages against semiconductor quantum dots, and these features that make them better alternatives for in vitro and in vivo bio-imaging [53, 54]. Also, while toxic heavy metals were using for the synthesis of semiconductor nanoparticles, it is possible and practicable to synthesize CDs from non-toxic sources. Nevertheless, the luminescence of CDs should be enhanced to achieve the luminescence of semiconductor based-quantum dots and CDs with higher quantum yields should be synthesized to compete with commercial alternatives [53, 55]. Meanwhile, the fluorescence behavior of CDs are sensitive to pH. Therefore, photoluminescence of CDs can switchable by changing pH [56]. Additionally, fluorescence ability of CDs provides sensing properties to CDs [57]. The applications in drug delivery and gene transfer by CDs also reported due to their transport capacity, and the fluorescence feature of CDs gives a chance to monitor the transfer process [57]. The opportunity of designing CDs as charge convertible gives them superior advantages for drug delivery like reducing the side effects by preventing the drug uptake by untargeted cells [58].

Nerium oleander (Oleander), is a member of the Apocynaceae family. It's a sempervirent toxic shrub with generally white or pink flowers and narrow long green leaves. The chemical constituents of *Nerium oleander* vary as cardiac glycosides, triterpenes, flavonoids glycosides and etc. [59–64]. Thermal synthesis of CDs is based on the principle of using saccharides and their derivatives as a carbon source. The polysaccharide content of Oleander seems to be proper for carbon nanodot synthesis. Besides, the effects of the carbon sources on CDs synthesis due to the chemical content of the plant extracts can vary depending on the solvent type used in the extraction step which needs to be investigated.

In this original research, the effects of the extract types and synthesis conditions on CDs structure were investigated in combination with the physical conditions of reaction media and the synthesis temperature. Two different Oleander extracts were utilized as carbon source, and CDs were thermally synthesized under various conditions considering pH, ionic strength and surface passivation agent addition to the reaction media for each combination of the extraction method and the synthesis temperature. The relationship among the investigated parameters and CDs features were evaluated by characterization studies using UV-Vis spectrophotometry, fluorescence spectrophotometry, Fourier transform infrared spectroscopy (FTIR) and dynamic light scattering analysis (DLS).

Experimental Study

Materials

Plant Material

Nerium oleander leaves were collected from Esenler, İstanbul (41° 01′ 37.7“ N, 28° 53’ 32.1” E) at 82 m, in May 2016 and were booked in Izmir, Ege University Faculty of Pharmacy Herbarium (IZEF) with number 6056.

Chemicals

Ethanol (EtOH), hydrochloric acid (HCl), sodium hydroxide (NaOH), sodium chloride (NaCl) and polyethylene glycol (PEG) 10,000 N were purchased from Sigma-Aldrich.

Equipments

Elma, TI-H 5 ultrasonic bath was used over the extraction process. Thermal synthesis of CDs was accomplished at Nuve muffle furnace. The characterization studies of CDs were performed at Shimadzu UV-1800 UV-Vis spectrophotometer, Agilent Cary Eclipse fluorescence spectrophotometer, Malvern Zeta Sizer Nano ZS, and Perkin Elmer Frontier FTIR.

Methods

Preparing Plant Extracts

Oleander fresh leaves were collected from nature, washed three times with distilled water and dried in an oven at 70 °C for two days. Dried leaves were ground to enhance their surface areas. Ethanol and water solvent extracts of Oleander leaves (12.5 g) were prepared in an ultrasonic bath at room temperature for 5 h with ethanol and ultra-pure water (100 mL), respectively. Finally, extracts were centrifuged at 5000 rpm for 15 min to remove redundant and clear extracts were kept at 4 °C.

CDs Synthesis

The preparations of PEG included and PEG free formulations of both extracts were represented in Fig. 1.

CDs were thermally synthesized in a muffle furnace for 45 min at various temperatures to investigate the effect of temperature on CDs formulation. After synthesis, residues in the crucibles were dissolved with 6 mL ultra-pure water and to obtain clear solutions, samples were centrifuged at 6000 rpm and 13,500 rpm for 20 min, respectively. Purified supernatants were kept at 4 °C. CDs were coded due to the extraction method (*E: ethanol, W: water*) and PEG inclusion as CD_E,

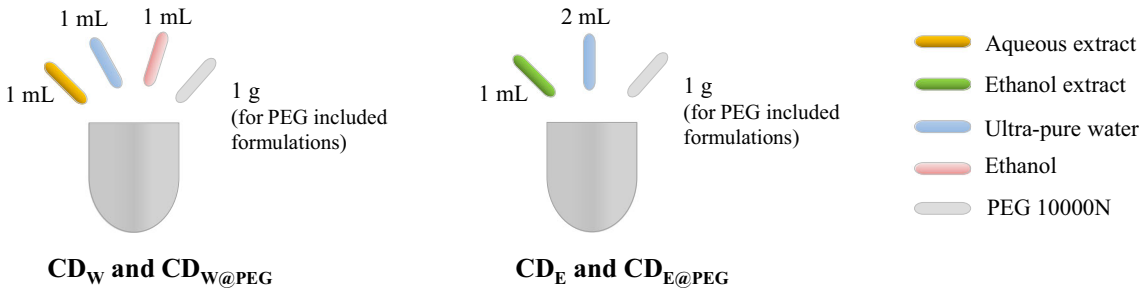

Fig. 1 Schematic view of CDs formulation

$CD_{E@PEG}$, CD_W, $CD_{W@PEG}$. In this case, CD_E represents CD synthesized from Oleander ethanol extract, $CD_{E@PEG}$ represents CD synthesized from Oleander ethanol extract in existence PEG, CD_W represents CD synthesized from Oleander aqueous extract and $CD_{W@PEG}$ represents CD synthesized from Oleander aqueous extract in existence PEG.

According to the hydrodynamic particle size, surface zeta potential and fluorescence feature of the particles; $CD_{E@PEG}$ and $CD_{W@PEG}$ synthesized at 300 °C were chosen for the evaluation of the impact of the other physical conditions on CDs formation (Fig. 2). To adjust pH and ionic strength of reaction media, 0.1 M HCl - 0.1 M NaOH solutions and in the range of 0–1 M NaCl solutions were used, respectively.

Characterization

Characterization studies were performed as reported Simsek et al. [52]. CDs samples were prepared by adding 50 μl of CDs solutions, mentioned in Section 2.2.2 which were stored at 4 °C, to 3 mL ultra-pure water. Optical characterization studies of CDs synthesized were performed by photoluminescence spectroscopy and the UV absorption spectra of CDs were recorded on a UV-spectrophotometer by using a 1 cm path length cuvette [65]. Fluorescence emitted from CDs were searched with a UV lamp at 365 nm wavelength. Particle size distribution and surface zeta potential of CDs synthesized were measured with DLS technique. About

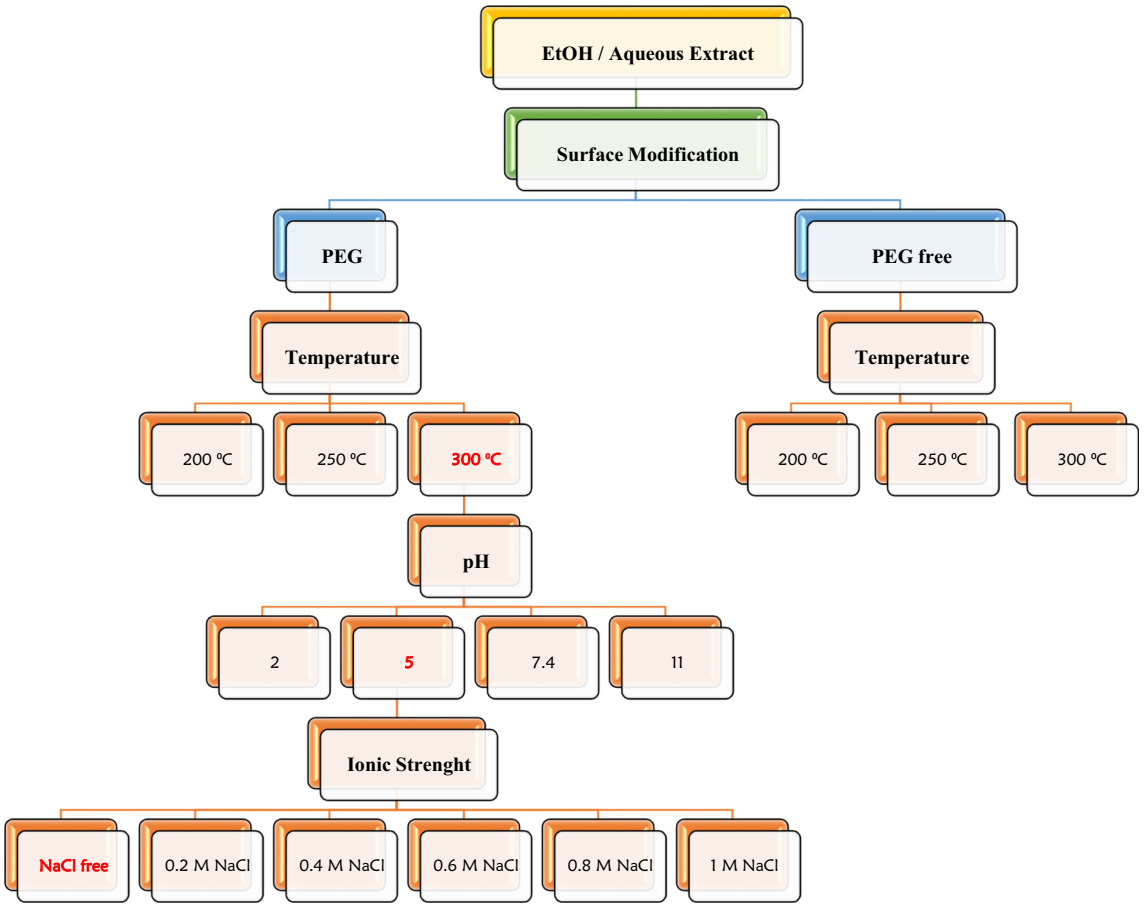

Fig. 2 Flow diagram of the present study

1 mL of CD solution was transferred to a disposable zeta cell, and the measurements were made in three replicates each with 12 zeta runs for particle size distribution. Mean particle size and standard deviations were calculated. Similarly, for surface zeta potential measurement, ~1 mL of CD solution was transferred in a disposable zeta cell. Three replicates each with 20 zeta runs were performed for analysis with dip cell. The FTIR spectrum of CDs with a resolution of 4 cm^{-1} was collected over the range of 450–4000 cm^{-1} on FTIR spectrometer. All measurements were performed in the ambient atmosphere and room temperature.

Results and Discussion

Effects of the Extract Types and Surface Passivation on CDs

Optic feature of nanoparticles can be investigated by UV-Vis spectroscopy [65]. Original carbon nanoparticles give a broad peak at 365 nm [66]. The peaks among 300–400 nm can be related with n-π* transition of C=O [41, 67–71] and peaks among 240 and 300 nm can be related to the π-π* transition based on C=C units [20, 41, 69, 70, 72, 73]. These original peaks at 240–300 nm and 300–400 nm were determined for all synthesized CDs (Supporting Information *Figure S1*). In comparison to PEG free formulations, the dramatic increases on absorption were observed for PEG included CDs (Fig. 3a). These increases at around 370 nm could be associated with the increase of surface energy level in CDs [74]. The effect of the extract types on the optical feature of CDs can be followed in **Figure S1**. In general, the UV-Vis profile of the particles were similar to each other with respect to extraction types. Other parameters investigated should be more effective than the extraction type on the optical features of CDs.

Fluorescence emissions were investigated at various excitation values in the range of 365–550 nm. Higher intensity values were mostly obtained at 365 nm excitation, and further studies were sustained at this excitation (Supporting Information *Figure S2*). Also, fluorescence luminescence of CDs was visualized under 365 nm UV light by the naked eye and photographed (Fig. 4). A strong relationship was determined between the fluorescence luminescence and PEG inclusion in the reaction media which can be explained with the surface passivation effect of PEG (Fig. 4, Supporting Information *Figure S3*) [3]. Also, the superior fluorescence values of the CDs mostly were obtained from ethanol extract originated CDs and the impact of the extraction types on the fluorescence feature was evinced (*Figure S3*).

Particle size has key importance on CDs photoluminescence feature and their applications in optoelectronics and biomedical [25, 75]. Hydrodynamic particle size was in the range of ~1 and 235 nm (Table 1) while increased temperature resulted in variations in size. Nevertheless, the average sizes of CDs were mostly determined under 50 nm. CDs synthesized in the presence of PEG showed smaller particle sizes than PEG free formulations. The size decreasing effects of surface modification were found compatible with the previous reports (Fig. 5) [76]. Besides, *Nerium oleander* aqueous extract based CDs showed smaller size than ethanol extract based ones in general, i.e. while PEG included formulations of aqueous extract $CD_{W@PEG}$ found as about 2 nm, ethanol extract based ones ($CD_{E@PEG}$) found as around 15 nm (Fig. 5a). This difference may be explained by the variety of chemical compounds in the extracts that act as a passivating agent which stabilize dangling surface groups. The main principle of the thermal process is condensation of

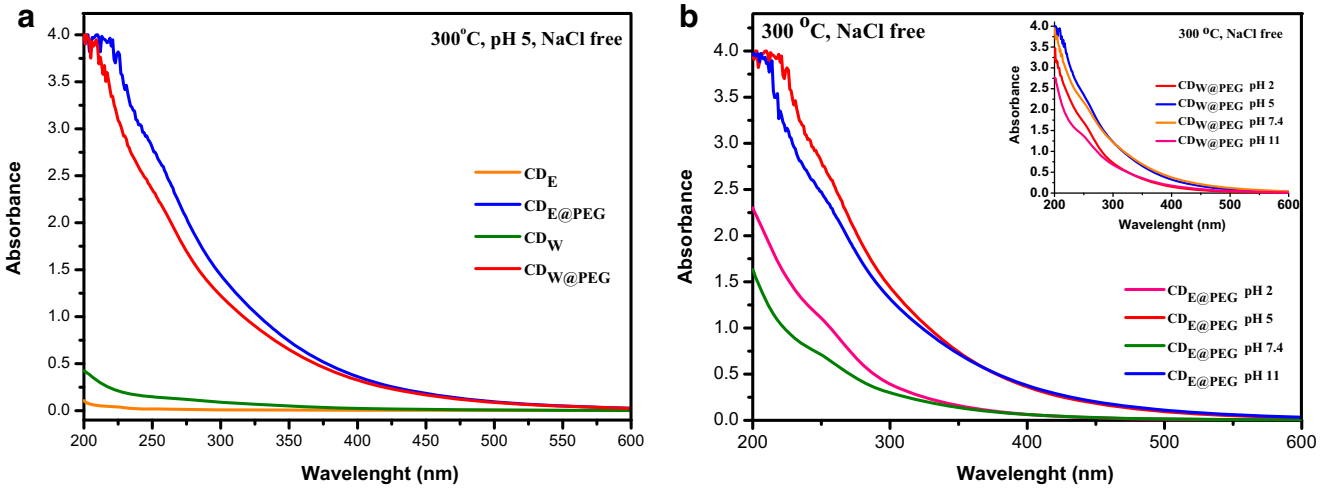

Fig. 3 UV-Vis spectra of CDs; **a** Effect of surface passivation agent, **b** Effect of pH

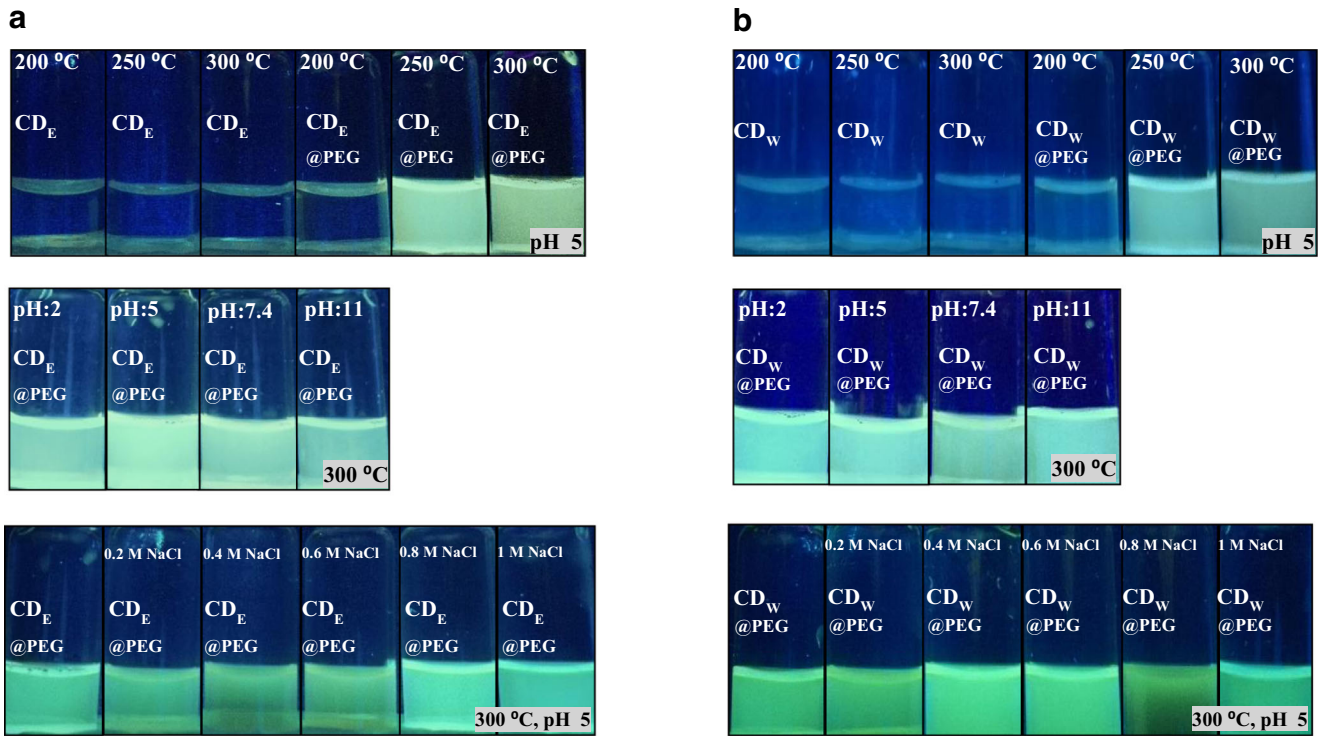

Fig. 4 Fluorescence luminescence of CDs under UV-light at 365 nm; **a** CD_E and $CD_{E@PEG}$ **b** CD_W and $CD_{W@PEG}$

the carbonaceous building blocks induced by high temperature and crystallization of the graphitic core [54]. Because of the higher polarity value of water than ethanol, the aqueous extract may have more saccharide derivatives than ethanol extract. The carbonization of the saccharide derivatives during thermal synthesis step may induce the formation of smaller particles.

The surface potential of all CDs was found as negatively charged, and the range of surface zeta potential was determined between −6 and −31 mV depending on the changes in physical conditions and carbon sources (Table 1, *Figure S5*). The surface zeta potential values of unmodified CDs with PEG were found to be decreased from −20.2 to −24.4 mV and from −28.4 to −31.1 mV for CD_E and CD_W, respectively, due to the temperature increase from 200 to 250 °C. But, CDs modified with PEG showed significant increases on the surface zeta potential values from −28.6 to −6.77 mV and from −21.2 to −11.6 mV for $CD_{E@PEG}$ and $CD_{W@PEG}$, respectively. The surface potential of aqueous extract based CDs had higher negativity on their surfaces than ethanol extract based ones while the overall average surface zeta potential of ethanol extract based CDs was calculated as −16.38 mV, aqueous extract based CDs' overall average surface zeta potential found as −21.10 mV. Under various pH values of reaction media, $CD_{E@PEG}$ may be qualified as having an increasing profile on the negativity of surface zeta potential till pH 7.4, and then, the surface zeta potential may be evaluated as stable with a small change. While surface zeta potential of $CD_{W@PEG}$ may be regarded as stable for pH 2, 5 and 11; a significant increase on the surface zeta potential at pH 7.4 was determined from −23.5 to −14.4 mV. For the effects of ionic strength of the reaction media on surface zeta potential of CDs, an increasing profile was observed except at 0.4 and 1 M NaCl concentrations for $CD_{E@PEG}$ and 0.4 and 0.8 M for $CD_{W@PEG}$. For the surface passivation agent inclusion to the reaction media, PEG free CDs were mostly found as more negatively charged due to the occurrence of the more acidic surface which is rich in –COOH. When the surface modified with PEG, the dangling bonds on the surface stabilized, and the number of carboxyl groups decreased due to the impact of surface passivation [3, 76]. It was reported by Shaik et al. [77] in their study that the negatively charged nanoparticles caused less DNA damage than the positively charged samples. Also, the surface potential of nanoparticles affects the cytotoxicity and the biophysicochemical interactions between nanoparticles and biological systems [78, 79]. Therefore, the reporting on the changes of the surface charges due to the variation in carbon source, surface passivation agent inclusion, reaction temperature and physical conditions of reaction media provides important know-how.

The change of the surface functional groups due to the parameters investigated was determined by FTIR spectra. While the general profile of FTIR spectra similar both for PEG free/PEG included formulations and extract types, minor

Table 1 Hydrodynamic particle size and surface zeta potential data of CDs

Formulation & Reaction Conditions			Hydrodynamic Particle Size (R_h) ± Std. Dev. (nm)	Average Surface Zeta Potential (-Pot) ± Std. Dev. (mV)	Conductivity (mS/cm)	Mob (μmcm/Vs)
CD_E	200 °C	pH 5	45.95 ± 6.84	−20.2 ± 1.92	0.0242	−1.58
	250 °C		148.85 ± 20.58	−24.4 ± 2.31	0.0239	−1.91
	300 °C		234.87 ± 31.15	−17.9 ± 5.67	0.0115	−1.403
$CD_{E@PEG}$	200 °C		15.88 ± 1.36	−28.6 ± 0.96	0.0256	−2.241
	250 °C		13.70 ± 1.24	−6.77 ± 1.32	0.1670	−0.5304
	300 °C		16.22 ± 1.33	−17.8 ± 0.42	0.0543	−1.392
CD_W	200 °C		3.07 ± 0.44	−28.4 ± 3.29	0.0310	−2.226
	250 °C		31.49 ± 2.23	−31.1 ± 1.75	0.0271	−2.441
	300 °C		22.86 ± 2.22	−25.7 ± 1.11	0.0243	−2.015
$CD_{W@PEG}$	200 °C		2.57 ± 0.35	−21.2 ± 1.72	0.0404	−1.659
	250 °C		1.99 ± 0.19	−11.6 ± 0.90	0.0714	−0.9059
	300 °C		2.05 ± 0.22	−23.5 ± 6.21	0.0499	−1.84
$CD_{E@PEG}$	300 °C	pH 2	32.46 ± 2.30	−14.7 ± 2.95	0.0560	−1.155
		pH 5	16.22 ± 1.33	−17.8 ± 0.42	0.0543	−1.392
		pH 7.4	44.48 ± 2.75	−25.1 ± 4.92	0.0260	−1.967
		pH 11	24.24 ± 1.72	−23.7 ± 1.29	0.0414	−1.863
$CD_{W@PEG}$		pH 2	1.06 ± 0.10	−25.4 ± 4.90	0.0349	−1.99
		pH 5	2.05 ± 0.22	−23.5 ± 6.21	0.0499	−1.84
		pH 7.4	2.40 ± 0.22	−14.4 ± 2.49	0.0319	−1.132
		pH 11	1.69 ± 0.17	−23.6 ± 6.21	0.0411	−1.853
$CD_{E@PEG}$	300 °C pH 5	NaCl free	16.22 ± 1.33	−17.8 ± 0.42	0.0543	−1.392
		0.2 M NaCl	12.7 ± 1.18	−12.8 ± 2.36	0.1550	−1.005
		0.4 M NaCl	11.98 ± 1.03	−14.8 ± 0.91	0.3200	−1.156
		0.6 M NaCl	11.68 ± 0.95	−9.34 ± 1.67	0.4520	−0.7334
		0.8 M NaCl	75.69 ± 4.99	−6.41 ± 0.70	0.5870	−0.055
		1.0 M NaCl	61.06 ± 5.53	−11.7 ± 1.04	0.7343	−0.9164
$CD_{W@PEG}$	300 °C pH 5	NaCl free	2.05 ± 0.22	−23.5 ± 6.21	0.0499	−1.84
		0.2 M NaCl	22.04 ± 1.77	−22.2 ± 4.71	0.1430	−1.743
		0.4 M NaCl	44.50 ± 4.43	−28.07 ± 1.44	0.3410	−2.2007
		0.6 M NaCl	3.77 ± 0.53	−11.17 ± 1.33	0.4480	−0.876
		0.8 M NaCl	21.46 ± 1.70	−17.9 ± 2.01	0.6570	−1.404
		1.0 M NaCl	2.3 ± 0.19	−6.33 ± 0.64	0.7350	−0.496

differences in peaks and/or intensities were observed for each condition (*Figure S6*). For example, all CDs at pH 5 had C-H stretching bands around 2880 and 2980 cm^{-1} at each synthesis temperature while the peaks were sharper for CD_W and $CD_{W@PEG}$ formulations than ethanol extract based CDs (*Figure S6*) [80–82]. The detailed analysis of surface functional groups can be followed in *Section 3.2* and *Section 3.3*.

After the evaluation of data collected from characterization studies of CDs which were synthesized from different carbon sources (ethanol and aqueous extracts of Oleander leaves) with or without surface passivation agent addition, it was decided to pursue the further studies with PEG included formulations of both carbon sources due to their fluorescence feature and smaller size (Fig. 2).

Effects of the Synthesis Temperatures on CDs

The effects of synthesis temperature on CDs formation can be followed from Supporting Information *Figure S1*. Strongly absorbed peaks at ~230 nm and ~290 nm were connected with the π-π* transition of the non-bonding electrons [65]. For PEG included CDs formulations, the increases observed on the absorbance at around 370 nm may be related with the increase of surface energy levels [74].

The only non-fluorescence CDs of PEG included formulations were observed at 200 °C. Lower temperatures were reported as carbonization ratio may be insufficient for the surface passivation of carbon quantum dots leading non-fluorescent particles [83]. While an increment was observed

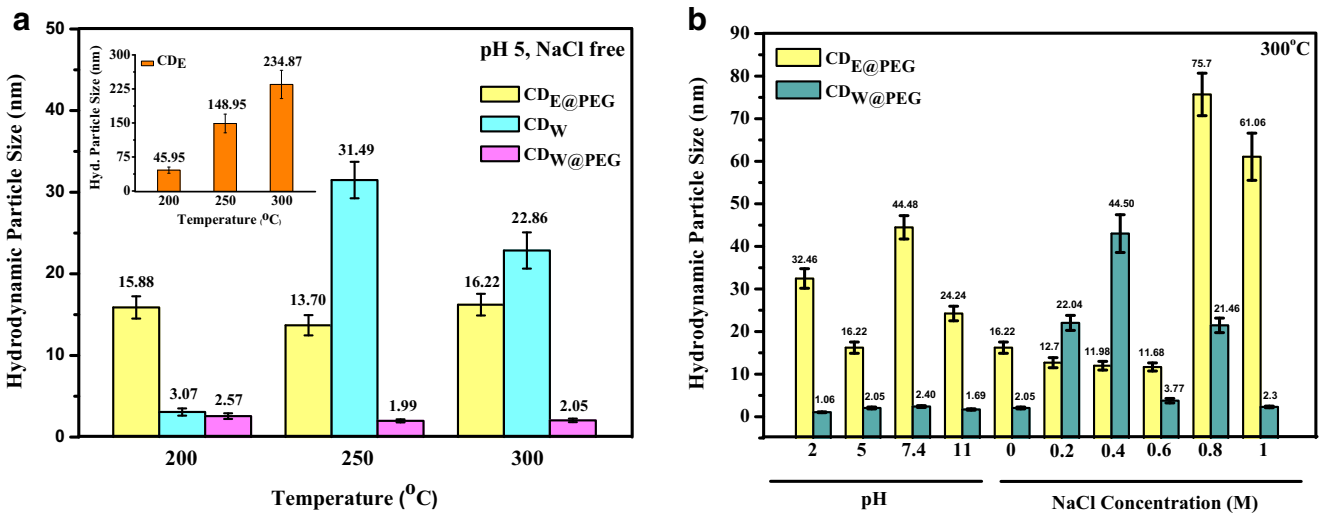

Fig. 5 Particle size distribution of CDs; **a** Effect of surface passivation agent, carbon source and synthesis temperature, **b** Effect of pH and ionic strength of the reaction media

on the fluorescence intensity of CDs with ascending temperature, the unexpected fluorescence behavior of CDs synthesized at 250 °C may be related with the aggregation of smaller particles (*Figure S3*) [83].

No apparent correlation with the hydrodynamic particle sizes and surface charges of CDs and synthesis temperature has been observed. Although, the impact of the synthesis temperature on the hydrodynamic particle size and surface zeta potential of CDs may be followed in Fig. 5a and *Figure S5*, respectively.

According to FTIR spectra of CDs given in *Figure S6*, in all temperatures, CDs showed stretching and bending pulse of $-CH_3$ and $-CH_2$ groups occurred at ~3000 cm^{-1} sharply and ~1400 cm^{-1} [82]. Reaction temperature did not show a significant impact on the surface functionalization of CDs in the case of usage of aqueous extract of Oleander as a carbon source (CD_W and $CD_{W@PEG}$). On the other hand, FTIR spectra of ethanol originated CDs (CD_E and $CD_{E@PEG}$) were same for 200 and 250 °C, a dramatic change on the surface was observed at 300 °C (*Figure S6*). O-H/N-H stretching peaks were identified at ~3660 cm^{-1} for CD_W, $CD_{W@PEG}$, $CD_{E@PEG}$ at different reaction temperatures, and H bonded –OH stretching at around 3200 cm^{-1} was observed for CD_E at 300 °C (*Figure S6*) [8, 48, 73, 80, 81, 84–86].

Taking account the results obtained, CDs synthesized at 300 °C were chosen for the further studies due to their smaller size and high fluorescence emission features.

Effects of pH and Ionic Strength

Effect of solution pH on the physicochemical properties of synthesized CDs was analyzed at the range of pH 2 and pH 11. According to the absorbance spectra of CDs due to the pH change of the reaction media, the increases on absorbance values at pH 5 and 11 were observed for $CD_{E@PEG}$. Similarly, for $CD_{W@PEG}$, at pH 5 and 7.4, absorbance values were higher than the others (Supporting Information *Figure S1*). These increases at around 370 nm can be associated with the increase of surface energy level in CDs [74]. Although no significant correlation between the ionic strength and absorbance was determined, the effect of pH on absorbance can be observed in Fig. 3b.

As can be seen in *Figure S3*, an alteration in the fluorescence intensity values due to the variation of physical conditions as pH and ionic strength of the reaction media was clearly observed. Even though, Goncalves et al. performed another procedure as using mercapto succinic acid to functionalization of carbon nanoparticles which were synthesized by laser ablation, the relevant changes obtained in our study on the fluorescence feature of CDs due to pH change were found compatible with their results [28]. The superior fluorescence intensities in the variety of pH and ionic strengths changes of the reaction media were obtained from the CDs at pH 5 and 2, and NaCl free and 0.4 M NaCl including medium for $CD_{E@PEG}$ and $CD_{W@PEG}$, respectively.

For the hydrodynamic particle sizes of CDs due to pH and ionic strength of the reaction media, a significant correlation between investigated parameters and CDs size could not be determined. However, the size distribution of the particles with respect to changes in pH and the ionic strength of the reaction media can be followed in Fig. 5b and *Fig. S4*.

Due to the change at the pH and ionic strength (for $CD_{W@PEG}$ from 0.6 M NaCl to 1 M) of the synthesis media, the aliphatic C-H bands disappeared (*Figure S8*). Stretching bands at around 1070, 1150, 1250 and 1370 cm^{-1} were attributed to asymmetric bridge oxygen and C-O vibrations (*Figures S7, S8*) [8, 10, 16, 38, 81, 86, 87]. For $CD_{E@PEG}$ at pH 2 and 7.4, C=O stretch, C-O stretch, and C-H bend were

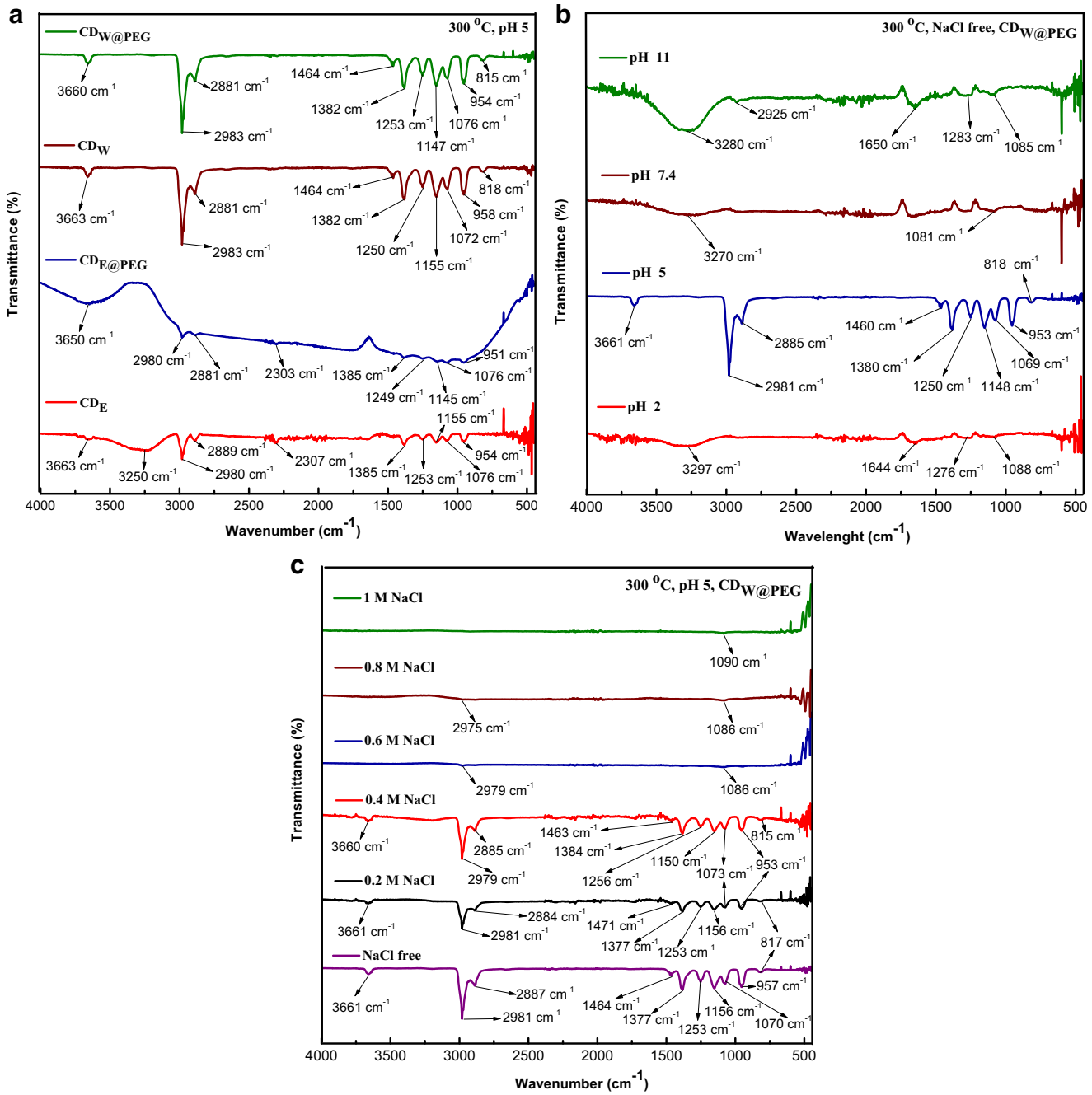

Fig. 6 FTIR spectra of CDs; **a** Effects of surface passivation agent and carbon source, **b** Effects of pH of the reaction media on $CD_{W@PEG}$ **c** Effects of ionic strength of the reaction media on $CD_{W@PEG}$

detected at ~1735, ~1215 and ~1360 cm^{-1}, respectively [48, 88]. At pH 5 and 11, while C=O band disappeared, O-H/N-H stretching peak formed at ~3660 cm^{-1}. Also, while C-O stretching between 1000 and 1300 cm^{-1} and C-H stretching at 2875 and 2982 cm^{-1} were observed at pH 5, for the same formulation, these peaks were missing at pH 11 (*Figure S7*) [84, 85]. For $CD_{W@PEG}$, while the FTIR profiles of the particles at pH 2, 7.4 and 11 were similar to each other, the surface functional groups were dramatically changed at pH 5. Such that for $CD_{W@PEG}$ synthesized at pH 5, O-H/N-H, C-H, C-O stretches were observed around 3661 cm^{-1}, 2891–2885 cm^{-1} and 1070–1380 cm^{-1}, respectively. However, $CD_{W@PEG}$ synthesized at the other pH values of reaction media, broad H bonded –OH stretching and weakening of C-O stretches were determined at about 3280 cm^{-1} and 1080–1280 cm^{-1}, respectively. For pH 2 and 11, C=C bending at 1645 cm^{-1} may be associated with the aromatic structures in CDs by combining the UV-Vis data which was indicated with π-π^* transition at around 260 nm (Fig. 4b, Fig. 6b) [84, 87]. Then, the existence of the aromatic structures in CDs may be discussed.

While investigating the effects of the variance on the ionic strength of reaction media on CDs, FTIR profiles of $CD_{E@PEG}$ at various ionic strengths were found similar to each other for 0.2 M NaCl to 1 M NaCl. $CD_{E@PEG}$ synthesized at various ionic strengths 0.2 M NaCl to 1 M NaCl showed C-O stretching between 1000 and 1400 cm^{-1}, C-H stretching at around 2880–2980 cm^{-1} and O-H/N-H stretching at around 3660 cm^{-1}, respectively. However, NaCl free formulations of $CD_{E@PEG}$ showed a little bit different FTIR profile. While C-O stretching between 1000 and 1400 cm^{-1} and C-H stretching at around 2880–2980 cm^{-1} peaks were weaker than the other formulations, broader O-H/N-H band was determined at 3637 cm^{-1} (*Figure S8*). For $CD_{W@PEG}$, up to 0.6 M NaCl inclusive formulations, O-H/N-H, and C-H stretching peaks were identified at ~3660 cm^{-1} and ~2880–2980 cm^{-1}, respectively. Nevertheless, for higher NaCl concentrations, almost all of the peaks disappeared or a significant weakening was determined for $CD_{W@PEG}$ formulations, and they may be defined as infrared inactive. This case may be related to polar bonds or asymmetrical molecules whose electrical dipole moment is zero (Fig. 6c) [87].

According to the data obtained from characterization studies of CDs synthesized at various pH, it was determined that CDs synthesized at pH 5 had a smaller particle size, and therefore, ionic strength studies were performed at pH 5. Similarly, the smaller hydrodynamic particle sizes were obtained from NaCl free formulations in general.

Conclusions

This original paper is the first report on the investigation of the effects of the solvents used in the extraction process and the synthesis conditions on CDs formation by using *Nerium oleander* leaves extracts as a carbon source. According to the findings, it was concluded that the extract type has considerable significance on the surface chemistry, size and surface zeta potential of carbon nanoparticles formed. Due to the extract types and synthesis conditions, nanoparticles smaller than 5 nm were successfully obtained. Besides, it was verified that the PEG addition in the reaction media has a great impact on the fluorescence feature of the particles. Moreover, the effects of the modifications on the synthesis conditions and formulations were examined to determine the CDs fluorescence feature and their physicochemical properties. Eventually, for the relevant extracts of Oleander, CDs synthesized from PEG included formulations at pH 5 and NaCl free reaction media seems like better alternatives than the CDs synthesized under other conditions taking account their effect on fluorescence feature, hydrodynamic particle size, and etc. Nevertheless, the surface charges of nanoparticles have great importance on cytotoxicity and the biophysicochemical interactions between nanoparticles and biological systems. Therefore, it will be better to choose any CDs due to their application purpose. Consequently, determining the relationship between the physical factors and CDs feature has importance due to the goal-directed synthesis of CDs for desired applications.

Acknowledgments Sinem Simsek gratefully acknowledges the Scientific and Technological Research Council of Turkey (TUBITAK) for the scholarship. Melis O. Alas also thanks to the Council of Higher Education of Turkey for the scholarship.

Compliance with Ethical Standards

Conflict of Interest The authors declare no conflicts of interest.

References

1. Wang J, Zhang Z, Zha S, Zhu Y, Wu P, Ehrenberg B, Chen JY (2014) Carbon nanodots featuring efficient FRET for two-photon photodynamic cancer therapy with a low fs laser power density. Biomaterials 35:9372–9381. https://doi.org/10.1016/j.biomaterials.2014.07.063
2. Sun YP, Zhou B, Lin Y, Wang W, Fernando KAS, Pathak P, Meziani MJ, Harruff BA, Wang X, Wang H, Luo PG, Yang H, Kose ME, Chen B, Veca LM, Xie SY (2006) Quantum-sized carbon dots for bright and colorful photoluminescence. J Am Chem Soc 128:7756–7757. https://doi.org/10.1021/ja062677d
3. Alas MO, Genc R (2017) An investigation into the role of macromolecules of different polarity as passivating agent on the physical, chemical and structural properties of fluorescent carbon nanodots. J Nanopart Res 19:185. https://doi.org/10.1007/s11051-017-3863-1
4. Xu X, Ray R, Gu Y, Ploehn HJ, Gearheart L, Raker K, Scrivens WA (2004) Electrophoretic analysis and purification of fluorescent singwalled carbon nanotube fragments. J Am Chem Soc 126:12736–12737. https://doi.org/10.1021/ja040082h
5. Roy P, Chen PC, Periasamy AP, Chen YN, Chang HT (2015) Photoluminescent carbon nanodots: synthesis, physicochemical properties and analytical applications. Mater Today 18:447–458. https://doi.org/10.1016/j.mattod.2015.04.005
6. Li J, Zhang L, Li P, Zhang Y, Dong C (2018) One step hydrothermal synthesis of carbon nanodots to realize the fluorescence detection of picric acid in real samples. Sensors Actuators B Chem 258:580–588. https://doi.org/10.1016/j.snb.2017.11.096
7. Gude V (2014) Synthesis of hydrophobic photoluminescent carbon nanodots by using L-tyrosine and citric acid through a thermal oxidation route. Beilstein J Nanotechnol 5:1513–1522. https://doi.org/10.3762/bjnano.5.164
8. Naghdi T, Atashi M, Golmohammadi H, Saeedi I, Alanezhad M (2017) Carbon quantum dots originated from chitin nanofibers as a fluorescent chemoprobe for drug sensing. J Ind Eng Chem 52:162–167. https://doi.org/10.1016/j.jiec.2017.03.039
9. Nafiujjaman M, Kim J, Park HK, Lee YK (2018) Preparation of blue-color-emitting graphene quantum dots and their in vitro and in vivo toxicity evaluation. J Ind Eng Chem 57:171–180. https://doi.org/10.1016/j.jiec.2017.08.019
10. Choi J, Kim N, Oh JW, Kim FS (2018) Bandgap engineering of nanosized carbon dots through electron-accepting functionalization. J Ind Eng Chem 65:104–111. https://doi.org/10.1016/j.jiec.2018.04.018
11. Li L, Zhao F, Zhang T, Lü C (2019) A facile method to prepare polymer functionalized carbon dots inspired by the mussel

chemistry for LED application. Dyes Pigments 162:845–854. https://doi.org/10.1016/j.dyepig.2018.11.015
12. Ma L, Xiang W, Gao H, Wang J, Ni Y, Liang X (2016) Facile synthesis of tunable fluorescent carbon dots and their third-order nonlinear optical properties. Dyes Pigments 128:1–7. https://doi.org/10.1016/j.dyepig.2016.01.005
13. Tao H, Yang K, Ma Z, Wan J, Zhang Y, Kang Z, Liu Z (2012) In vivo NIR fluorescence imaging, biodistribution, and toxicology of photoluminescent carbon dots produced from carbon nanotubes and graphite. Small 8:281–290. https://doi.org/10.1002/smll.201101706
14. Zhang X, Zhang Y, Wang Y, Kalytchuk S, Kershaw SV, Wang Y, Wang P, Zhang T, Zhao Y, Zhang H, Cui T, Wang Y, Zhao J, Yu WW, Rogach AL (2013) Color-switchable electroluminescence of carbon dot light-emitting diodes. ACS Nano 7:11234–11241. https://doi.org/10.1021/nn405017q
15. Paulo S, Palomares E, Martinez-Ferrero E (2016) Graphene and carbon quantum dot-based materials in photovoltaic devices: from synthesis to applications. Nanomaterials 6:157. https://doi.org/10.3390/nano6090157
16. De B, Voit B, Karak N (2014) Carbon dot reduced cu $_2$ O nanohybrid/hyperbranched epoxy nanocomposite: mechanical, thermal and photocatalytic activity. RSC Adv 4:58453–58459. https://doi.org/10.1039/C4RA11120F
17. Guo D-Y, Shan C-X, Qu S-N, Shen D-Z (2014) Highly sensitive ultraviolet photodetectors fabricated from ZnO quantum dots/carbon Nanodots hybrid films. Sci Rep 4:7469. https://doi.org/10.1038/srep07469
18. Yang C-H, Yen C-C, Jheng J-J, Wang CY, Chen SS, Huang PY, Huang KS, Shaw JF (2015) Correction: Yang, C.-H., et al. immobilization of Brassica oleracea Chlorophyllase 1 (BoCLH1) and Candida rugosa lipase (CRL) in magnetic alginate beads: an enzymatic evaluation in the corresponding proteins. Molecules 2014, 19, 11800-11815. Molecules 20:7325–7328. https://doi.org/10.3390/molecules20047325
19. Jayaraman T, Murthy AP, Elakkiya V, Chandrasekaran S, Nithyadharseni P, Khan Z, Senthil RA, Shanker R, Raghavender M, Kuppusami P, Jagannathan M, Ashokkumar M (2018) Recent development on carbon based heterostructures for their applications in energy and environment: a review. J Ind Eng Chem 64:16–59. https://doi.org/10.1016/j.jiec.2018.02.029
20. Pandey S, Gedda GR, Thakur M, Bhaisare ML, Talib A, Khan MS, Wu SM, Wu HF (2017) Theranostic carbon dots 'clathrate-like' nanostructures for targeted photo-chemotherapy and bioimaging of cancer. J Ind Eng Chem 56:62–73. https://doi.org/10.1016/j.jiec.2017.06.008
21. Liu X, Wang T, Wang W, Zhou Z, Yan Y (2018) A tailored molecular imprinting ratiometric fluorescent sensor based on red/blue carbon dots for ultrasensitive tetracycline detection. J Ind Eng Chem 72:100–106. https://doi.org/10.1016/j.jiec.2018.12.007
22. Myint AA, Rhim WK, Nam JM, Kim J, Lee YW (2018) Water-soluble, lignin-derived carbon dots with high fluorescent emissions and their applications in bioimaging. J Ind Eng Chem 66:387–395. https://doi.org/10.1016/j.jiec.2018.06.005
23. Jiang R, Huang Q, Tian J et al (2019) Ultrafast fabrication of fluorescent organic nanoparticles with aggregation-induced emission feature through the microwave-assisted Biginelli reaction. Dyes Pigments 165:90–96. https://doi.org/10.1016/j.dyepig.2019.01.056
24. Suda Y, Ono T, Akawaza M et al (2002) Preparation of carbon nanoparticles by plasma-assisted pulsed laser deposition method—size and binding energy dependence on ambient gas pressure and plasma condition. Thin Solid Films 415:15–20. https://doi.org/10.1016/S0040-6090(02)00532-1
25. Li H, Kang Z, Liu Y, Lee ST (2012) Carbon nanodots: synthesis, properties and applications. J Mater Chem 22:24230–24253. https://doi.org/10.1039/c2jm34690g
26. Cao L, Wang X, Meziani MJ, Lu F, Wang H, Luo PG, Lin Y, Harruff BA, Veca LM, Murray D, Xie SY, Sun YP (2007) Carbon dots for multiphoton bioimaging. J Am Chem Soc 129:11318–11319. https://doi.org/10.1021/ja073527l
27. Miao P, Han K, Tang Y, Wang B, Lin T, Cheng W (2015) Recent advances in carbon nanodots: synthesis, properties and biomedical applications. Nanoscale 7:1586–1595. https://doi.org/10.1039/c4nr05712k
28. Gonçalves H, Da Silva JCGE (2010) Fluorescent carbon dots capped with PEG200and mercaptosuccinic acid. J Fluoresc 20:1023–1028. https://doi.org/10.1007/s10895-010-0652-y
29. Zhao Q-L, Zhang Z-L, Huang B-H, Peng J, Zhang M, Pang DW (2008) Facile preparation of low cytotoxicity fluorescent carbon nanocrystals by electrooxidation of graphite. Chem Commun:5116–5118. https://doi.org/10.1039/b812420e
30. Wang X, Long Y, Wang Q, Zhang H, Huang X, Zhu R, Teng P, Liang L, Zheng H (2013) Reduced state carbon dots as both reductant and stabilizer for the synthesis of gold nanoparticles. Carbon N Y 64:499–506. https://doi.org/10.1016/j.carbon.2013.07.104
31. Xie Z, Wang F, Liu CY (2012) Organic-inorganic hybrid functional carbon dot gel glasses. Adv Mater 24:1716–1721. https://doi.org/10.1002/adma.201104962
32. Li H, He X, Liu Y, Huang H, Lian S, Lee ST, Kang Z (2011) One-step ultrasonic synthesis of water-soluble carbon nanoparticles with excellent photoluminescent properties. Carbon N Y 49:605–609. https://doi.org/10.1016/j.carbon.2010.10.004
33. Costas-Mora I, Romero V, Lavilla I, Bendicho C (2014) In situ building of a nanoprobe based on fluorescent carbon dots for methylmercury detection. Anal Chem 86:4536–4543. https://doi.org/10.1021/ac500517h
34. Wang F, Wang S, Sun Z, Zhu H (2015) Study on ultrasonic single-step synthesis and optical properties of nitrogen-doped carbon fluorescent quantum dots. Fullerenes Nanotub Carbon Nanostructures 23:769–776. https://doi.org/10.1080/1536383X.2014.996287
35. Krysmann MJ, Kelarakis A, Dallas P, Giannelis EP (2012) Formation mechanism of carbogenic nanoparticles with dual photoluminescence emission. J Am Chem Soc 134:747–750. https://doi.org/10.1021/ja204661r
36. Guo Y, Zhang L, Cao F, Leng Y (2016) Thermal treatment of hair for the synthesis of sustainable carbon quantum dots and the applications for sensing Hg2+. Sci Rep 6:1–7. https://doi.org/10.1038/srep35795
37. Liu Y, Zhao Y, Zhang Y (2014) One-step green synthesized fluorescent carbon nanodots from bamboo leaves for copper(II) ion detection. Sensors Actuators B Chem 196:647–652. https://doi.org/10.1016/j.snb.2014.02.053
38. Fadllan A, Marwoto P, Aji MP, et al (2017) Synthesis of carbon nanodots from waste paper with hydrothermal method. In: AIP conference proceedings. p 030069
39. Zhu H, Wang X, Li Y, Wang Z, Yang F, Yang X (2009) Microwave synthesis of fluorescent carbon nanoparticles with electrochemiluminescence properties. Chem Commun:5118–5120. https://doi.org/10.1039/b907612c
40. Liu H, He Z, Jiang LP, Zhu JJ (2015) Microwave-assisted synthesis of wavelength-tunable photoluminescent carbon nanodots and their potential applications. ACS Appl Mater Interfaces 7:4913–4920. https://doi.org/10.1021/am508994w
41. Choi Y, Thongsai N, Chae A, Jo S, Kang EB, Paoprasert P, Park SY, in I (2017) Microwave-assisted synthesis of luminescent and biocompatible lysine-based carbon quantum dots. J Ind Eng Chem 47:329–335. https://doi.org/10.1016/j.jiec.2016.12.002
42. Mohamad NAN, Jai J, Arham NA, Hadi A (2013) A short review on the synthesis of bimetallic nanoparticles using plant extract. In: 2013 IEEE international conference on control system, computing and engineering. pp 334–339

43. Kavitha K, Baker S, Rakshith D et al (2013) Plants as green source towards synthesis of nanoparticles. Int Res J Biol Sci 2:66–76
44. Shah M, Fawcett D, Sharma S, et al (2015) Green synthesis of metallic nanoparticles via biological entities
45. Varisco M, Zufferey D, Ruggi A, Zhang Y, Erni R, Mamula O (2017) Synthesis of hydrophilic and hydrophobic carbon quantum dots from waste of wine fermentation. R Soc Open Sci 4. https://doi.org/10.1098/rsos.170900
46. Phadke C, Mewada A, Dharmatti R, Thakur M, Pandey S, Sharon M (2015) Biogenic synthesis of fluorescent carbon dots at ambient temperature using Azadirachta indica (neem) gum. J Fluoresc 25: 1103–1107. https://doi.org/10.1007/s10895-015-1598-x
47. Mewada A, Pandey S, Shinde S, Mishra N, Oza G, Thakur M, Sharon M, Sharon M (2013) Green synthesis of biocompatible carbon dots using aqueous extract of Trapa bispinosa peel. Mater Sci Eng C 33: 2914–2917. https://doi.org/10.1016/j.msec.2013.03.018
48. Liu H, Ding L, Chen L, Chen Y, Zhou T, Li H, Xu Y, Zhao L, Huang N (2018) A facile, green synthesis of biomass carbon dots coupled with molecularly imprinted polymers for highly selective detection of oxytetracycline. J Ind Eng Chem 69:455–463. https://doi.org/10.1016/j.jiec.2018.10.007
49. Bano D, Kumar V, Singh VK, Hasan SH (2018) Green synthesis of fluorescent carbon quantum dots for the detection of mercury(ii) and glutathione. New J Chem 42:5814–5821. https://doi.org/10.1039/c8nj00432c
50. Bhatt S, Bhatt M, Kumar A, Vyas G, Gajaria T, Paul P (2018) Green route for synthesis of multifunctional fluorescent carbon dots from Tulsi leaves and its application as Cr(VI) sensors, bio-imaging and patterning agents. Colloids Surfaces B Biointerfaces 167:126–133. https://doi.org/10.1016/j.colsurfb.2018.04.008
51. Bayat A, Masoum S, Hosseini ES (2019) Natural plant precursor for the facile and eco-friendly synthesis of carbon nanodots with multifunctional aspects. J Mol Liq 281:134–140. https://doi.org/10.1016/j.molliq.2019.02.074
52. Simsek S, Alas MÖ, Ozbek B et al (2019) Evaluation of the physical properties of fluorescent carbon Nanodots synthesized using Nerium oleander extracts by microwave-assisted synthesis methods (accepted manuscript). J Mater Res Technol xx:1–14. https://doi.org/10.1016/j.jmrt.2019.04.008
53. Lim SY, Shen W, Gao Z (2015) Carbon quantum dots and their applications. Chem Soc Rev 44:362–381. https://doi.org/10.1039/C4CS00269E
54. Jelinek R (2017) Carbon quantum dots. Springer International Publishing, Cham
55. Kargbo O, Jin Y, Ding S-N (2015) Recent advances in luminescent carbon dots. Curr Anal Chem 11:4–21. https://doi.org/10.2174/1573411010666141010160217
56. Qu JH, Wei Q, Sun DW (2018) Carbon dots: principles and their applications in food quality and safety detection. Crit Rev Food Sci Nutr 58:2466–2475. https://doi.org/10.1080/10408398.2018.1437712
57. Tuerhong M, XU Y, YIN XB (2017) Review on carbon dots and their applications. Chin J Anal Chem 45:139–150. https://doi.org/10.1016/S1872-2040(16)60990-8
58. Xiao L, Sun H (2018) Novel properties and applications of carbon nanodots. Nanoscale Horizons 3:565–597. https://doi.org/10.1039/c8nh00106e
59. Sharma P, Choudhary AS, Parashar P et al (2010) Chemical constituents of plants from the genus Nerium. Chem Biodivers 7:1198–1207. https://doi.org/10.1002/cbdv.200900172
60. Sinha SN, Biswas K (2016) A concise review on *Nerium oleander* L . - an important medicinal plant. 3:408–412
61. Bai L, Wang L, Zhao M, Toki A, Hasegawa T, Ogura H, Kataoka T, Hirose K, Sakai J, Bai J, Ando M (2007) Bioactive pregnanes from Nerium oleander. J Nat Prod 70:14–18. https://doi.org/10.1021/np068030o
62. Begum S, Sultana R, Siddiqui BS (1997) Triterpenoids from the leaves of Nerium oleander. Phytochemistry 44:329–332
63. Siddiqui BS, Khatoon N, Begum S, Farooq AD, Qamar K, Bhatti HA, Ali SK (2012) Flavonoid and cardenolide glycosides and a pentacyclic triterpene from the leaves of Nerium oleander and evaluation of cytotoxicity. Phytochemistry 77:238–244. https://doi.org/10.1016/j.phytochem.2012.01.001
64. Bai L, Zhao M, Toki A, Sakai JI, Yang XY, Bai Y, Ando M, Hirose K, Ando M (2010) Three new cardenolides from methanol extract of stems and twigs of Nerium oleander. Chem Pharm Bull 58:1088–1092. https://doi.org/10.1248/cpb.58.1088
65. Edison TNJI, Atchudan R, Sethuraman MG, Shim JJ, Lee YR (2016) Microwave assisted green synthesis of fluorescent N-doped carbon dots: cytotoxicity and bio-imaging applications. J Photochem Photobiol B Biol 161:154–161. https://doi.org/10.1016/j.jphotobiol.2016.05.017
66. Song Y, Kang X, Zuckerman NB, Phebus B, Konopelski JP, Chen S (2011) Ferrocene-functionalized carbon nanoparticles. Nanoscale 3:1984–1989. https://doi.org/10.1039/c0nr00953a
67. Hu S, Trinchi A, Atkin P, Cole I (2015) Tunable photoluminescence across the entire visible spectrum from carbon dots excited by white light. Angew Chem Int Ed 54:2970–2974. https://doi.org/10.1002/anie.201411004
68. Lai Q, Zhu S, Luo X, Zou M, Huang S (2012) Ultraviolet-visible spectroscopy of graphene oxides. AIP Adv 2:3–8. https://doi.org/10.1063/1.4747817
69. Carata E, Anna Tenuzzo B, Arnò F, Buccolieri A, Serra A, Manno D, Dini L (2012) Stress response induced by carbon nanoparticles in Paracentrotus lividus. Int J Mol Cell Med 1:30–38
70. De B, Karak N (2013) A green and facile approach for the synthesis of water soluble fluorescent carbon dots from banana juice. RSC Adv 3:8286–8290. https://doi.org/10.1039/c3ra00088e
71. Zhao Y, Liu X, Yang Y, Kang L, Yang Z, Liu W, Chen L (2015) Carbon dots: from intense absorption in visible range to excitation-independent and excitation-dependent photoluminescence. Fullerenes Nanotub Carbon Nanostructures 23:922–929. https://doi.org/10.1080/1536383X.2015.1018413
72. Bourlinos AB, Trivizas G, Karakassides MA, Baikousi M, Kouloumpis A, Gournis D, Bakandritsos A, Hola K, Kozak O, Zboril R, Papagiannouli I, Aloukos P, Couris S (2015) Green and simple route toward boron doped carbon dots with significantly enhanced non-linear optical properties. Carbon N Y 83:173–179. https://doi.org/10.1016/j.carbon.2014.11.032
73. Liu X, Pang J, Xu F, Zhang X (2016) Simple approach to synthesize amino-functionalized carbon dots by carbonization of chitosan. Sci Rep 6:31100. https://doi.org/10.1038/srep31100
74. Isnaeni RI, Intan R, Zakaria M (2018) Photoluminescence study of carbon dots from ginger and galangal herbs using microwave technique. J Phys Conf Ser 985:0–6. https://doi.org/10.1088/1742-6596/985/1/012004
75. Baker SN, Baker GA (2010) Luminescent carbon nanodots: emergent Nanolights. Angew Chem Int Ed 49:6726–6744. https://doi.org/10.1002/anie.200906623
76. Sonthanasamy RSA, Fazry S, Yamin BM, Lazim AM (2018) Surface functionalization of highly luminescent carbon nanodots from Dioscorea hispida with polyethylene glycol and branched polyethyleneimine and their in vitro study. J King Saud Univ - Sci. https://doi.org/10.1016/j.jksus.2018.05.004
77. Sultana Shaik A, Pasha Shaik A, Al Faraj A, Bammidi VK (2018) Effect of polyethylene glycol surface charge functionalization of SWCNT on the in vitro and in vivo Nanotoxicity and biodistribution monitored noninvasively using MRI. Toxicol Mech Methods 0:1–41. https://doi.org/10.1080/15376516.2018.1540674

78. Liu X, Li H, Jin Q, Ji J (2014) Surface tailoring of nanoparticles via mixed-charge monolayers and their biomedical applications. Small 10:4230–4242. https://doi.org/10.1002/smll.201401440
79. Tatur S, MacCarini M, Barker R et al (2013) Effect of functionalized gold nanoparticles on floating lipid bilayers. Langmuir 29: 6606–6614. https://doi.org/10.1021/la401074y
80. De B, Voit B, Karak N (2014) Carbon dot reduced Cu2O nanohybrid/hyperbranched epoxy nanocomposite: mechanical, thermal and photocatalytic activity. RSC Adv 4:58453–58459. https://doi.org/10.1039/c4ra11120f
81. De B, Kumar M, Mandal BB, Karak N (2015) An in situ prepared photo-luminescent transparent biocompatible hyperbranched epoxy/carbon dot nanocomposite. RSC Adv 5:74692–74704. https://doi.org/10.1039/c5ra12131k
82. Nie H, Li M, Li Q, Liang S, Tan Y, Sheng L, Shi W, Zhang SXA (2014) Carbon dots with continuously tunable full-color emission and their application in ratiometric pH sensing. Chem Mater 26: 3104–3112. https://doi.org/10.1021/cm5003669
83. Milosavljevic V, Moulick A, Kopel P, et al Milosazljevic, V., Moulick, A., Kopel, P., Adam, V., & Kizek, R. 2014. 16–22
84. Li W, Yue Z, Wang C, Zhang W, Liu G (2013) An absolutely green approach to fabricate carbon nanodots from soya bean grounds. RSC Adv 3:20662–20665. https://doi.org/10.1039/c3ra43330g
85. Himaja AL, Karthik PS, Sreedhar B, Singh SP (2014) Synthesis of carbon dots from kitchen waste: conversion of waste to value added product. J Fluoresc 24:1767–1773. https://doi.org/10.1007/s10895-014-1465-1
86. Gupta A, Verma NC, Khan S, Nandi CK (2016) Carbon dots for naked eye colorimetric ultrasensitive arsenic and glutathione detection. Biosens Bioelectron 81:465–472. https://doi.org/10.1016/j.bios.2016.03.018
87. Ţucureanu V, Matei A, Avram AM (2016) FTIR spectroscopy for carbon family study. Crit Rev Anal Chem 46:502–520. https://doi.org/10.1080/10408347.2016.1157013
88. Fadllan A, Marwoto P, Aji MP et al (2017) Synthesis of carbon nanodots from waste paper with hydrothermal method. AIP Conf Proc 1788. https://doi.org/10.1063/1.4968322